

Convolutional Bypasses Are Better Vision Transformer Adapters

Shibo Jie, Zhi-Hong Deng

School of Artificial Intelligence, Peking University
parsley@pku.edu.cn, zhdeng@pku.edu.cn

Abstract

The pretrain-then-finetune paradigm has been widely adopted in computer vision. But as the size of *Vision Transformer* (ViT) grows exponentially, the full finetuning becomes prohibitive in view of the heavier storage overhead. Motivated by *parameter-efficient transfer learning* (PETL) on language transformers, recent studies attempt to insert lightweight adaptation modules (e.g., adapter layers or prompt tokens) to pretrained ViT and only finetune these modules while the pretrained weights are frozen. However, these modules were originally proposed to finetune language models. Although ported well to ViT, their design lacks prior knowledge for visual tasks. In this paper, we propose to construct *Convolutional Bypasses* (Convpass) in ViT as adaptation modules, introducing only a small amount (less than 0.5% of model parameters) of trainable parameters to adapt the large ViT. Different from other PETL methods, Convpass benefits from the hard-coded inductive bias of convolutional layers and thus is more suitable for visual tasks, especially in the low-data regime. Experimental results on VTAB-1k benchmark and few-shot learning datasets demonstrate that Convpass outperforms current language-oriented adaptation modules, demonstrating the necessity to tailor vision-oriented adaptation modules for vision models.

1 Introduction

Pretraining on large-scale datasets (e.g., ImageNet) and then fully finetuning on downstream tasks has become the de-facto paradigm to achieve state-of-the-art (SOTA) performance on visual tasks (Kolesnikov et al. 2020). However, this paradigm is not storage-efficient – it requires one to store a whole model for each downstream task. Recently, as *Vision Transformer* (ViT) (Dosovitskiy et al. 2021) dominates vision field gradually, the size of vision models has grown exponentially (58M of ResNet-152 (He et al. 2016) v.s. 1843M of ViT-G (Zhai et al. 2022)), which creates the demand for *parameter-efficient transfer learning* (PETL) on ViT.

Fortunately, since transformer was first adopted in *neural language processing* (NLP) (Vaswani et al. 2017), PETL on large pretrained language models has been studied sufficiently (Houlsby et al. 2019; Hu et al. 2022; Li and Liang 2021; He et al. 2022a), which can be easily ported to ViT.

Code: <https://github.com/JieShibo/PETL-ViT>

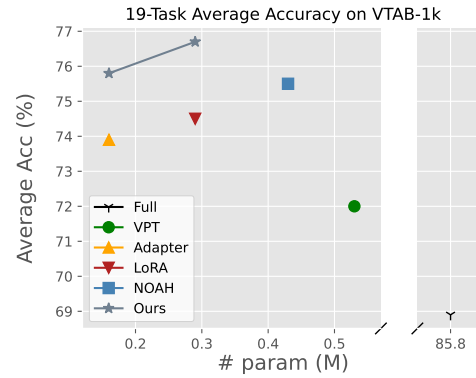


Figure 1: **Average accuracy v.s. number of trainable parameters on VTAB-1k benchmark.** Our vision-oriented Convpass outperforms other language-oriented methods.

Concretely, these PETL methods insert lightweight adaptation modules into the pretrained models, freeze the pretrained weights, and finetune these modules end-to-end to adapt to downstream tasks. Recent work has verified the effectiveness of these PETL methods on ViT (Jia et al. 2022; Zhang, Zhou, and Liu 2022), but we raise the question: *Are these modules designed for the language models optimal for the vision models as well?*

It is known that NLP and visual tasks desire different inductive bias, which profoundly affects the model architecture design. By analyzing current PETL methods from an unraveled perspective, we argue that these methods, called “language-oriented modules”, also imply the inductive bias for language, e.g., weak spatial relation and support for variable-length input. Therefore, a better adaptation module for ViT should also reflect visual inductive bias, such as spatial locality and 2D neighborhood structure, which is referred to as “vision-oriented modules”.

When a model (e.g., ViT) has weak inductive bias, it needs a large amount of data to learn the inductive bias from scratch. That may not be a serious problem in the pretraining process, since we can leverage easily accessible unlabeled data for self-supervised learning (Bao, Dong, and Wei 2022; He et al. 2022b), or resort to multi-modal pretraining (Radford et al. 2021; Yu et al. 2022). However, data

of downstream tasks is usually collected from specific domains, which may be expensive or hard to acquire. Although the model has learned some of such inductive bias during pretraining, a well-designed vision-oriented PETL module would improve data efficiency much further.

In this paper, we propose to construct *Convolutional Bypasses* (Convpss) in ViT as adaptation modules. Convpss is an inserted convolutional bottleneck block parallel to the MHSA or MLP block, which “bypasses” the original ViT block. It reconstructs the spatial structure of the token sequence and performs convolution on image tokens and `[cls]` token individually. During finetuning, only these Convpss blocks and the classification head are updated. Due to the hard-coded locality of convolutional layers, Convpss can capture visual information more efficiently, especially when the downstream data is limited. As shown in Figure 1, Convpss only introduces and tunes about 0.29M new parameters for a ViT-B of 86M, while achieving better performance than both full finetuning and current SOTA language-oriented methods on 19-task VTAB benchmark (Zhai et al. 2019). Further experiments on few-shot learning demonstrate that Convpss also outperforms other baselines in the low-data regime, and can be directly used on vision-language model (Radford et al. 2021) with good domain generalization performance.

We summarize the contributions as follows:

- We point out the weak visual inductive bias of current PETL methods.
- We propose Convpss, a simple but effective PETL methods which leverages trainable convolutional blocks as bypasses to adapt pretrained ViT to downstream visual tasks.
- Experimental results show that Convpss outperforms previous language-oriented methods, emphasizing the necessity to tailor vision-oriented adaptation modules for vision models.

2 Related Work

2.1 Vision Transformer

Transformer-based models have achieved great success in NLP (Devlin et al. 2019; Raffel et al. 2020; Brown et al. 2020). ViT adopts this architecture in visual tasks by partitioning the images into patches which are embedded and flattened into 1D token sequences.

In ViT, each layer consists of two kinds of blocks: *Multi-Head Self-Attention* (MHSA) and *Multi-Layer Perceptron* (MLP). In an MHSA block, the input sequence $\mathbf{X} \in \mathbb{R}^{N \times d}$ is firstly projected to query $\mathbf{Q} = \mathbf{X}\mathbf{W}_q$, key $\mathbf{K} = \mathbf{X}\mathbf{W}_k$, and value $\mathbf{V} = \mathbf{X}\mathbf{W}_v$, respectively, in which $\mathbf{W}_{q/k/v} \in \mathbb{R}^{d \times d}$. They are further divided into N_h heads: $\{\mathbf{Q}^{(i)}\}_{i=1}^{N_h}, \{\mathbf{K}^{(i)}\}_{i=1}^{N_h}, \{\mathbf{V}^{(i)}\}_{i=1}^{N_h}$. Then, the self-attention of a single head is formulated as

$$\text{Attn-Head}^{(i)}(\mathbf{X}) = \text{Softmax} \left(\frac{\mathbf{Q}^{(i)} \mathbf{K}^{(i)\top}}{\sqrt{d}} \right) \mathbf{V}^{(i)}$$

The outputs of all heads are further concatenated and linearly projected as the outputs of the MHSA block.

An MLP block consists of two fully-connected (FC) layers, whose weights are $\mathbf{W}_1 \in \mathbb{R}^{d \times D}$ and $\mathbf{W}_2 \in \mathbb{R}^{D \times d}$, respectively. Ignoring the bias parameters for simplicity, the MLP is formulated as

$$\text{MLP}(\mathbf{X}) = \text{GELU}(\mathbf{X}\mathbf{W}_1)\mathbf{W}_2$$

Since ViT has much less visual inductive bias, it performs worse than its convolutional counterparts (e.g., ResNet) when the training data is not sufficient. For this reason, some recent works propose to introduce inductive bias into ViT (Liu et al. 2021b; Wu et al. 2021), which significantly reduce its dependency on scale of dataset. But on the other hand, since vanilla ViT shares the same backbone as the transformer-based language models, it can leverage current SOTA multi-modal pretraining methods with a vast amount of auto-annotated image-text pairs (Wang et al. 2021; Yu et al. 2022). Therefore, we still focus on PETL on vanilla ViT architecture, but propose to introduce hard-coded inductive bias by adaptation modules during finetuning instead of pretraining.

2.2 Parameter-Efficient Transfer Learning

PETL aims at using a small number of trainable parameters to adapt large models to downstream tasks. We here introduce four commonly used PETL methods in ViT.

Adapter (Houlsby et al. 2019; Pfeiffer et al. 2021) is a bottleneck MLP block composed of two fully connected layers, whose weights are $\mathbf{W}_{down} \in \mathbb{R}^{d \times h}$ and $\mathbf{W}_{up} \in \mathbb{R}^{h \times d}$, where $h \ll d$. Adapters are inserted into networks as residual connections, i.e., given an input $\mathbf{X} \in \mathbb{R}^{N \times d}$, the computation is formulated as

$$\mathbf{X} \leftarrow \mathbf{X} + \text{GELU}(\mathbf{X}\mathbf{W}_{down})\mathbf{W}_{up}$$

Pfeiffer et al. (2021) propose to place Adapters after the MLP blocks, which has been proven to be an efficient design in previous literature (Hu et al. 2022), so we follow this setting in this paper. Besides the above design, Chen et al. (2022) also propose a parallel Adapter to adapt MLP blocks for visual tasks.

LoRA (Hu et al. 2022) learns the low-rank approximation of increments of \mathbf{W}_q and \mathbf{W}_v . Formally, it decomposes $\Delta\mathbf{W}_{q/v}$ into $\mathbf{A}_{q/v}\mathbf{B}_{q/v}$, where $\mathbf{A}_{q/v} \in \mathbb{R}^{d \times r}, \mathbf{B}_{q/v} \in \mathbb{R}^{r \times d}$ and $r \ll d$. The query and key are computed as

$$\mathbf{Q}/\mathbf{K} = \mathbf{X}\mathbf{W}_{q/k} + s \cdot \mathbf{X}\mathbf{A}_{q/k}\mathbf{B}_{q/k}$$

in which s is a scaling hyperparameter.

VPT (Jia et al. 2022) has a similar idea with P-Tuning v2 (Liu et al. 2021a). It concatenates the input \mathbf{X} with several trainable prompts $\mathbf{P} \in \mathbb{R}^{l \times d}$ before each layer. This extended sequence is formulated as

$$\mathbf{X} \leftarrow [\mathbf{X}, \mathbf{P}]$$

These prompts are then cut apart at the end of a layer, and the prompts for the next layer are concatenated.

NOAH (Zhang, Zhou, and Liu 2022) is a newly proposed PETL method for ViT, which combines the above three module together and performs neural architecture search on

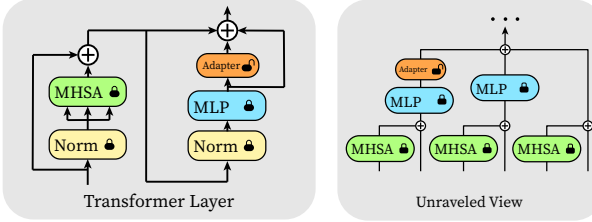


Figure 2: **Illustration of the unraveled view of a ViT layer equipped with Adapter.** The ViT can be viewed as an ensemble of these paths. Normalization layers are omitted for simplicity.

hidden dimension h of Adapter, rank r of LoRA, and prompt length l of VPT.

Note that although VPT and NOAH are proposed for visual tasks, their components are ported from NLP in essence. Therefore, all aforementioned PETL methods can be classified as language-oriented methods.

3 Methodology

3.1 Rethinking Adapters from an Unraveled View

Since Adapters and MHSA/MLP blocks all contain skip connections, we can unravel the ViT and rewrite it as a collection of paths. [Veit, Wilber, and Belongie \(2016\)](#) point out that the original network can be regarded as an ensemble of unraveled paths, so we here give a look at these paths to analyze the property of the original network.

As shown in Figure 2, a ViT equipped with Adapters can be viewed as an ensemble of three types of paths: **(Type I)** Frozen paths, which only contain MHSA/MLP blocks of the ViT. These paths are not trainable, and the sum of their outputs is identically equal to the output of the pretrained ViT. **(Type II)** MHSA-Adapter paths, where all MHSA blocks come before the first Adapter. **(Type III)** Adapter-MHSA paths, where at least one MHSA block is placed after an Adapter.

Finetuning the Adapters is equivalent to fitting the changes of outputs by the paths of **Type II & III**. In **Type II** paths, given the same input, the output tokens of the last MHSA blocks are unchanged, and there is no information exchange between tokens after that. Therefore, only the **Type III** paths, in fact, make changes to the token mixer of the pretrained ViT.

In a **Type III** paths, we can treat all Adapters and MLP blocks before an MHSA block as a part of its query/key-/value transformation, i.e., complicate these transformations from linear mapping to

$$Q/K/V = f_{q/k/v}(X)$$

where f is a channel-wise MLP. Therefore, finetuning **Type III** paths can be considered as finetuning the MHSA with complicated query/key/value transformations.

Meanwhile, since LoRA finetuning $W_{q/v}$ in a low-rank subspace and VPT can be regarded as parallel and gated Adapters ([He et al. 2022a](#)), all these language-oriented methods reckon on tuning MHSA to fulfill token mixer’s

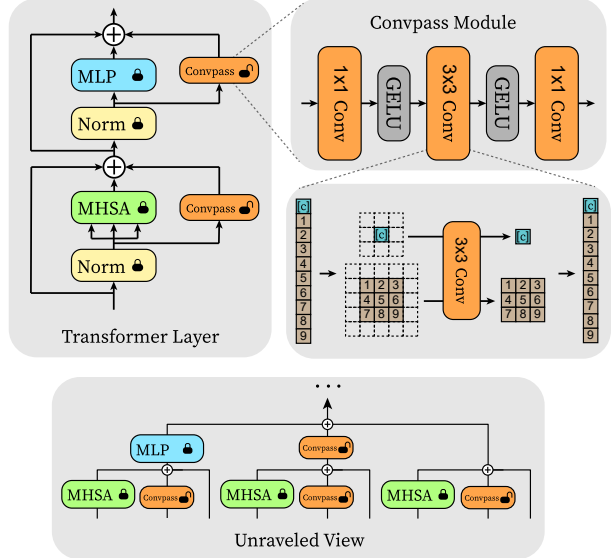


Figure 3: **Overview of our method.** We restore the spatial structure of the token sequence, and use trainable ResNet-style convolutional blocks as bypasses. The $[\text{cls}]$ token is regarded as an individual image.

role in downstream tasks. MHSA, however, lacks visual inductive bias, which may perform poorly when the data of downstream tasks is limited.

3.2 Adapting ViT via Convolutional Bypasses

Recent studies on modifying the architecture of ViT have verified that introducing convolution into ViT will improve the performance when training data is not adequate ([Dosovitskiy et al. 2021](#); [Wu et al. 2021](#)). Since the data of downstream tasks is usually limited even few-shot, we can also introduce convolution into the adaptation modules for PETL.

As illustrated in Figure 3, a Conpass module consists of three convolutional layers: an 1×1 convolution reducing the channel, a 3×3 convolution with the same input and output channel, and an 1×1 convolution expanding the channel. Since ViT flattens the image into an 1D token sequence, we restore the 2D structure before convolution. The $[\text{cls}]$ token serves as an individual image. The Conpass modules are placed parallel to the MHSA/MLP blocks, which can be formulated as

$$X \leftarrow X + \text{MHSA/MLP}(LN(X)) + s \cdot \text{Conpass}(LN(X))$$

where s is a hyperparameter and LN is Layer Normalization ([Ba, Kiros, and Hinton 2016](#)). Note that the Conpass modules are similar to the *residual bottleneck blocks* of ResNet ([He et al. 2016](#)). If we ignore the MHSA/MLP blocks, the ViT will turn into a ResNet-like CNN.

From the unraveled view, we can find that in each transformer layer, besides the frozen paths, there are also trainable paths that only contain Conpass or contain both Conpass and MHSA, which act as token-mixers. Therefore, the original transformer layers are converted to an ensemble of transformers, ResNet-like CNNs, and hybrid models. Since

# param (M)	Natural						Specialized				Structured										
	Cifar100	Caltech101	DTD	Flower102	Pets	SVHN	Sun397	Camelyon	EuroSAT	Resisc45	Retinopathy	Clevr-Count	Clevr-Dist	DMLab	KITTI-Dist	dSpr-Loc	dSpr-Ori	sNORB-Azim	sNORB-Ele	Average	
<i>Traditional Finetuning</i>																					
Full	85.8	68.9	87.7	64.3	97.2	86.9	87.4	38.8	79.7	95.7	84.2	73.9	56.3	58.6	41.7	65.5	57.5	46.7	25.7	29.1	68.9
Linear	0	64.4	85.0	63.2	97.0	86.3	36.6	51.0	78.5	87.5	68.5	74.0	34.3	30.6	33.2	55.4	12.5	20.0	9.6	19.2	57.6
<i>Homogeneous PETL methods</i>																					
VPT	0.53	78.8	90.8	65.8	98.0	88.3	78.1	49.6	81.8	96.1	83.4	68.4	68.5	60.0	46.5	72.8	73.6	47.9	32.9	37.8	72.0
Adapter	0.16	69.2	90.1	68.0	98.8	89.9	82.8	54.3	84.0	94.9	81.9	75.5	80.9	65.3	48.6	78.3	74.8	48.5	29.9	41.6	73.9
LoRA	0.29	67.1	91.4	69.4	98.8	90.4	85.3	54.0	84.9	95.3	84.4	73.6	82.9	69.2	49.8	78.5	75.7	47.1	31.0	44.0	74.5
Convpass-attn	0.16	71.5	90.7	71.9	99.2	91.1	90.3	54.2	83.2	95.6	83.8	74.6	81.1	64.5	50.8	81.0	86.8	52.5	35.4	43.1	75.8
Convpass	0.33	71.6	90.5	72.1	99.2	91.0	90.2	54.4	84.7	96.0	84.0	75.5	81.8	68.0	50.5	81.0	84.9	53.2	37.2	43.8	76.3
<i>Heterogeneous PETL methods</i>																					
NOAH	0.43	69.6	92.7	70.2	99.1	90.4	86.1	53.7	84.4	95.4	83.9	75.8	82.8	68.9	49.9	81.7	81.8	48.3	32.8	44.2	75.5
Convpass-MS	0.29	72.4	90.7	72.1	99.2	91.1	91.0	54.9	85.8	96.0	84.4	75.5	82.2	68.0	50.8	81.6	86.8	53.2	37.2	43.8	76.7

Table 1: **Full results on the VTAB-1k benchmark.** Classification heads are not taken into account in # param. The average results are averaged over three group-wise averages in Figure 4. Convpass(-attn) achieves 11 SOTA results out of the 19 tasks among homogeneous PETL methods, and Convpass-MS achieves 13 SOTA results among heterogeneous PETL methods.

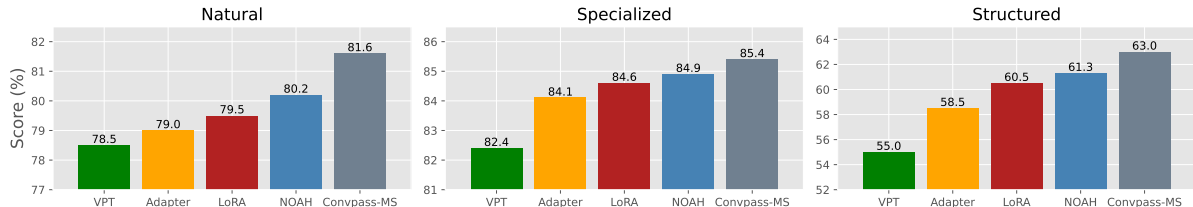


Figure 4: **Group-wise average results on VTAB-1k.** Convpass outperforms other baselines in all of the three groups.

all trainable paths contain Convpass modules, the finetuning process can benefit from the inherent 2D neighborhood structure of the 3×3 convolution.

If the bottleneck channel (i.e., the input & output channel of the 3×3 convolution) is denoted as h , and the amount of ViT layers is L , the number of trainable parameters is $2L \times ((2h+1)d + 9h^2 + 2h)$. In view of $h \ll d$ (e.g., $d = 768, h = 8$ in our experiments), this amount is $\mathcal{O}(Ld)$, which is negligible compared to ViT’s $\mathcal{O}(Ld^2)$ parameters.

4 Experiments

4.1 Transfer Learning on VTAB-1k Benchmark

First of all, our method is evaluated on the basic transfer learning scenario – finetuning the pretrained models on various downstream tasks.

Datasets To evaluate the performance on transfer learning of our methods, we use VTAB-1k (Zhai et al. 2019) as a benchmark. VTAB-1k benchmark contains 19 image classification tasks from different fields, which can be roughly categorized into three groups: Natural, Specialized, and Structured. Each classification task only has 1,000 training samples, which are split into a training set (800) and a validation set (200) during hyperparameter search. The reported test

set results are produced by the model trained on all 1,000 training samples.

Baselines We compare our method with two traditional finetuning methods: **Full** finetuning, which optimizes all parameters end-to-end; **Linear** evaluation, which freezes the pretrained backbone and only learns a classification head; as well as four PETL methods: **VPT**, **Adapter**, **LoRA**, and **NOAH**. For our method **Convpass**, we also report a simplified variant: **Convpass-attn**, which only inserts the Convpass modules alongside the MHSA blocks. For a clear comparison, we further categorize the PETL methods into two groups: VPT, Adapter, LoRA, and Convpass are **Homogeneous PETL methods** which only contain one type of PETL module, and the network architecture is the same for all tasks; NOAH is a **Heterogeneous PETL method** which focuses on architecture search to combine other existing PETL modules, resulting in a dynamic network architecture.

To fully explore the capacity of Convpass, we use a simple model selection strategy to construct a heterogeneous PETL method for comparison to NOAH. To be specific, we use the validation set to select one of the following three candidates for each task: Convpass, Convpass-attn, and **Convpass-hybrid**, which replaces the Convpass module

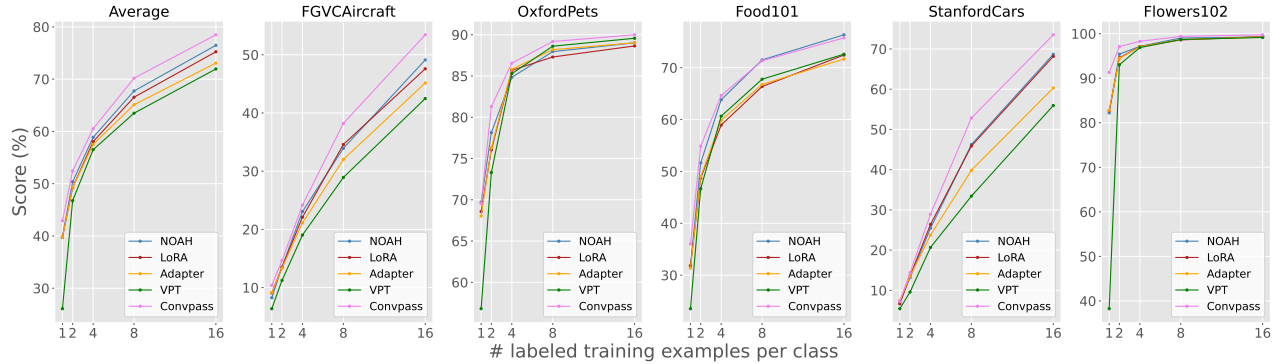


Figure 5: Results of few-shot learning on five fine-grained visual recognition datasets. Convpss outperforms other baselines on average results.

alongside each MLP block with an parallel Adapter module (see Section 4.4 for details). When using Convpss-attn and Convpss-hybrid with fewer 3×3 convolution, the model will rely more on MHSA, which potentially benefits shape-dominated tasks such as SVHN because MHSA is shape-bias while convolution is texture-bias (Park and Kim 2022). Therefore, the model selection actually adjusts the ratio of MHSA and convolution. After model selection, we retrain the model on the full training set and report the test set results. We call this heterogeneous PETL method **Convpss-MS**.

Setup For all methods, we use a ViT-B/16 (Dosovitskiy et al. 2021) supervisedly pretrained on ImageNet-21k (Deng et al. 2009). For all methods except for NOAH, the networks are finetuned for 100 epochs. NOAH also trains a supernet for another 500 epochs. The hidden dimension h of Adapter and Convpss, as well as the rank r of LoRA are all set to 8. The prompt length l of VPT follows the best recipe in the original paper. The hyperparameter s of Convpss is roughly searched in $\{0.01, 0.1, 1, 10, 100\}$. In this setting, Adapter and Convpss-attn have similar numbers of trainable parameters, while the Convpss’s trainable parameters are slightly more than LoRA’s but fewer than VPT’s.

Results As shown in Table 1, Convpss-attn outperforms its counterpart Adapter in 15 out of the 19 tasks, while Convpss and Convpss-MS outperform their counterparts LoRA and NOAH in 13 tasks, respectively. Although using fewer parameters, Convpss still performs better than VPT in 15 tasks. The PETL methods are all better than full finetuning overall. Because of the variety of tasks, no one method achieves SOTA on all tasks at once, but Convpss-MS achieves the best average performance, 1.2% higher than the SOTA PETL methods, NOAH. It is also worth noting that Convpss-attn also has better average results than NOAH, with only 40% number of parameters.

Figure 4 shows that Convpss-MS has the best performance in all the three groups of VTAB, indicating that Convpss-MS specializes in visual tasks from various domains. The superiority of Convpss is significant in the Natural and Structured groups. In the Specialized group, Con-

vpss does not remarkably outperform NOAH.

4.2 Few-Shot Learning

Few-shot learning is a common scenario when the data of downstream tasks is hard to obtain, and there are only a few training samples for each task that can be utilized.

Datasets We use five fine-gained datasets to evaluate the performance of our methods on few-shot learning: **FGVC-Aircraft** (Maji et al. 2013a), **Oxford-Pets** (Parkhi et al. 2012), **Food-101** (Bossard, Guillaumin, and Gool 2014), **Stanford Cars** (Krause et al. 2013), and **Oxford-Flowers102** (Nilsback and Zisserman 2006). We conduct experiments on 1, 2, 4, 8, and 16 shot settings. The results are averaged over three runs with different seeds. The baselines and experimental setup are the same as for VTAB-1k, but we only use the original Convpss as in Figure 3 in these experiments.

Results As shown in Figure 5, the average results of Convpss in the five settings are all higher than the other baselines. On FGVC-Aircraft and Stanford Cars, the advantages of Convpss are highlighted. On simpler Oxford-Pets and Oxford-Flowers102, all methods have similar performance, while Convpss is still in the lead. On Food-101, Convpss slightly under-performs NOAH in the 16-shot case, but the trend is reversed when the number of training data gets smaller. These results demonstrate that the introduced inductive bias of Convpss enhances ViT’s ability to learn in the low-data regime.

4.3 Domain Generalization

Besides vision models, PETL has been studied in the field of vision-language models as well. Considering the outstanding domain generalization property of vision-language models, we also evaluate the performance of our method under domain shift when applied to vision-language models.

Datasets In domain generalization experiments, the models are trained on the source domain, and tested on both the source and target domain. We use **ImageNet-1k** (Deng et al. 2009) as the source domain, where each class contains 16

Method	Source	Target			
		-V2	-Sketch	-A	-R
ZS CLIP	66.73	60.83	46.15	47.77	73.96
LP CLIP	65.85	56.26	34.77	35.68	58.43
CoOp	71.51	64.20	47.99	49.71	75.21
CoCoOp	71.02	64.07	48.75	50.63	76.18
Conpass	74.01	66.49	49.01	49.84	78.07

Table 2: **Results of 16-shot ImageNet classification and domain generalization on CLIP.** We report top-1 accuracy. Conpass outperforms the baselines in source domain and three of the four target domains.

training samples. The target domains include: **ImageNet-V2** (Recht et al. 2019), which is a new ImageNet test set collected with the original labelling protocol; **ImageNet-Sketch** (Wang et al. 2019), which consists of sketch images of the 1,000 ImageNet classes; **ImageNet-A** (Hendrycks et al. 2021b), which contains real-world adversarial samples of 200 of the ImageNet classes; **ImageNet-R** (Hendrycks et al. 2021a), which is composed of renditions of 200 ImageNet classes.

Baselines The CLIP (Radford et al. 2021) model consists of an image encoder and a text encoder, which are pretrained via contrastive learning on image-text pairs. Our method is compared with the following baselines: **Zero-Shot (ZS)** CLIP uses prompted label texts (e.g., ‘‘A photo of <class name>.’’) as the text encoder inputs, and classifies the images based on cosine similarity between image and text features; **Linear Probe (LP) CLIP** discards the text encoder and learns a linear classification head for image encoder; **CoOp** (Zhou et al. 2021) makes use of trainable vectors as prompts of labels; **CoCoOp** (Zhou et al. 2022) learns a meta-net to generate prompts of labels from images. Note that CoOp and CoCoOp are PETL methods designed for CLIP specifically.

To apply our methods to CLIP, we make the following modifications. **First**, we insert Conpass modules into the image encoder only, while the text encoder stays unchanged. **Second**, we add a FC layer as classification head of the image encoder, whose bias is zero-initialized and whose weight is initialized with encoded prompted label texts of all classes (just as in ZS CLIP). Then, the text encoder is discarded, and only the Conpass modules and head are finetuned.

Setup In our experiments, all methods use a ViT-B/16 as the image encoder, and a BERT-like (Devlin et al. 2019) model as the text encoder. For our methods, we train the Conpass modules and classification heads for 50 epochs.

Results The results are shown in Table 2. Our method, though not designed for CLIP, still remarkably outperforms the baselines tailored for CLIP in the source domain. In three out of the four target domains, Conpass also achieves SOTA performance. On ImageNet-A, Conpass performs a bit poorly, which is probably because the ImageNet-A dataset is collected by selecting samples misclassified by ResNet. Since Conpass modules are ResNet-style blocks,

Model	Method	Avg.	Nat.	Spe.	Str.
ConvNeXt-B	Full	74.0	78.0	83.7	60.4
ConvNeXt-B	Linear	63.6	74.5	81.5	34.8
Swin-B	Full	75.0	79.2	86.2	59.7
Swin-B	Linear	62.6	73.5	80.8	33.5
Swin-B	VPT	71.6	76.8	84.5	53.4
Swin-B	Conpass	77.2	82.9	86.9	61.9
ViT-B/16	Full	68.9	75.9	83.4	47.6
ViT-B/16	Linear	57.6	68.9	77.2	26.8
ViT-B/16	VPT	72.0	78.5	82.4	55.0
ViT-B/16	Conpass	76.3	81.3	85.1	62.6

Table 3: **Results on VTAB-1k.** ConvNeXt-B and Swin-B have inherent inductive bias for vision, while ViT introduces such inductive bias via Conpass during finetuning. Avg.: Average, Nat.: Natural, Spe.: Specialized, Str.: Structured.

they may be more easily misled by these samples as well. Overall, the results prove that Conpass is robust under domain shift.

4.4 Further Analyses

Comparison with Other Backbones One of the motivations for designing Conpass is to introduce visual inductive bias to ViT during finetuning. However, since there are also ViT variants (e.g., Swin Transformer (Liu et al. 2021b)) which have already incorporated visual inductive bias into their model designs, finetuning on these models can naturally benefit from such prior knowledge. Then a question arises: *Will the models which acquire inductive bias during finetuning outperform the models born with it?*

We conduct comparisons among the three backbone models: **ViT-B/16**, **Swin-B** (Liu et al. 2021b), and **ConvNeXt-B** (Liu et al. 2022). All of them are pretrained on ImageNet-21k and have a similar size. As the results shown in Table 3, when using traditional transfer learning methods (Full and Linear), Swin-B and ConvNeXt-B perform significantly better than ViT-B/16 as expected, which indicates the pivotal role of visual inductive bias during finetuning. However, when equipped with Conpass, the average performance of ViT-B/16 overtakes Swin-B and ConvNeXt-B. These observations suggest that Conpass is a proven and effective method to complement the missing inductive bias for downstream transfer.

Moreover, we also apply Conpass to Swin. Similarly, Conpass modules bypass the W-MHSA/SW-MHSA/MLP blocks of Swin, but we do not mask the inputs as the windowed attention does. As shown in Table 3, the advantage of Conpass over full finetuning still holds on Swin, but VPT is no longer competitive. This observation demonstrates that Conpass is a reliable PETL method performing constantly well on various backbone networks. From the comparison between Swin and ViT we also find that the improvement made by Conpass diminishes on Swin. This is also expected because the demand for supplementing visual inductive on Swin is not as pressing as on ViT.

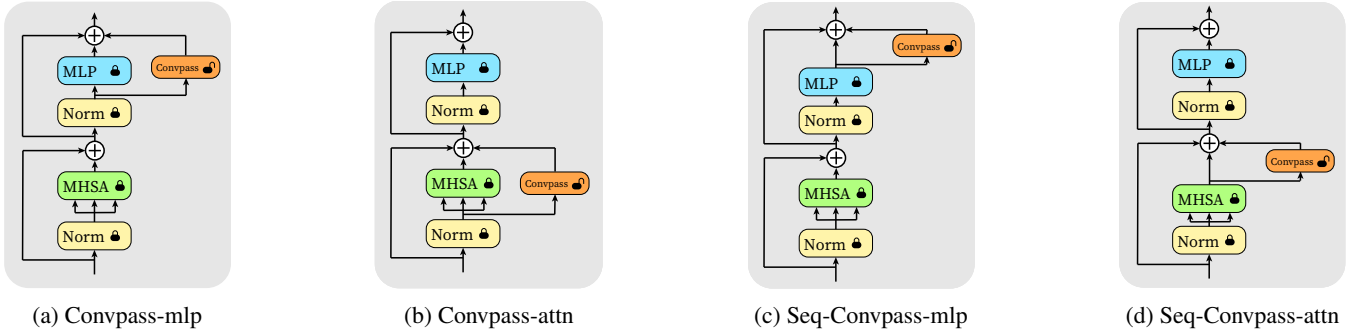


Figure 6: Four ways to insert a Convplass module into ViT.

Method	Avg.	Nat.	Spe.	Str.
<i>One adaptation module per layer</i>				
Adapter	73.9	79.0	84.1	58.5
Seq-Convplass-mlp	74.5	80.0	83.6	59.9
Seq-Convplass-attn	74.9	80.6	84.1	60.0
Convplass-mlp	75.4	80.3	84.5	61.2
Convplass-attn [†]	75.8	81.3	84.3	61.9
<i>Two adaptation modules per layer</i>				
Par-Adapter	75.2	81.3	84.6	59.6
Convplass-hybrid [†]	76.0	81.5	85.2	61.2
Convplass [†]	76.3	81.3	85.1	62.6

Table 4: **Results on VTAB-1k.** We find that (i) parallel is superior to sequential; (ii) alongside MHSA is superior to alongside MLP; and (iii) vision-oriented is superior to language-oriented. [†]: the best three models as candidates for Convplass-MS. : vision-oriented methods.

Where to Place the Convplass Modules Our Convplass modules are parallel to the MHSA/MLP blocks, but there is another choice: insert the modules after the MHSA/MLP blocks in a sequential way like Adapter. To figure out what is the optimal way to place the Convplass modules, we consider four forms when only one Convplass module is inserted in each ViT layer, as illustrated in Figure 6. **Convplass-mlp** and **Convplass-attn** are parallel Convplass modules alongside the MLP and MHSA blocks, while **Seq-Convplass-mlp** and **Seq-Convplass-attn** follow the MLP and MHSA blocks, respectively.

As shown in Table 4, we evaluate these designs on VTAB-1k, and find the following. **First**, the parallel designs are better than their sequential counterparts. From Figure 2, we know that the sequential modules add longer paths to the model, which are relatively harder to optimize with a small amount of downstream data. On the contrary, the parallel Convplass serve as shortcuts for better gradient propagation, and introduce fully-convolutional ResNet-like paths that do not exist in sequential designs. **Second**, we also find that placing the Convplass modules beside/after MHSA blocks is better than beside/after MLP blocks. Since Convplass-attn and Convplass-mlp are the best two designs, our Convplass is composed of them, i.e., placing Convplass modules along-

side both MHSA and MLP blocks in parallel.

Vision-Oriented v.s. Language-Oriented Finally, we conduct a ablation study on the vision-oriented idea, using two ablation models for comparison: **Convplass-hybrid**, as described in Section 4.1, which uses parallel Adapters instead of Convplass modules alongside the MLP blocks; and **Par-Adapter**, which uses parallel Adapters alongside both MHSA and MLP blocks. Such parallel Adapters for MLP blocks have been adopted by Chen et al. (2022) as well. As shown in Table 4, on average results, Convplass performs the best and Convplass-hybrid is better than Par-Adapter. Convplass-hybrid is slightly better than Convplass on Natural and Specialized results, but performs significantly worse on Structured tasks. Par-Adapter, though has similar result to Convplass on Natural tasks, lags behind on Specialized and Structured. Since the Structured tasks are about obtaining the structure of a scene (e.g., object counting or 3D depth prediction), they fairly differ from the pretraining tasks (i.e., ImageNet classification) and require more modifications to the pretrained token mixer. Therefore, the Structured tasks are more complicated and the superiority of vision-oriented modules is highlighted. The comparison between Adapter and Seq-Convplass-mlp also confirms this tendency.

In summary, the language-oriented Par-Adapter performs worse than the vision-oriented Convplass and Convplass-hybrid, supporting our standpoint. Since Convplass, Convplass-hybrid, and Convplass-attn are the best three models in Table 4, we choose them to serve as candidates for Convplass-MS for model selection.

5 Conclusion

In this paper, we point out that current PETL methods used in ViT lack inductive bias for visual tasks, which potentially degrades downstream finetuning performance. For this reason, we propose Convplass, a vision-oriented PETL method that constructs trainable convolutional bypasses to adapt pretrained ViT. Experimental results on VTAB-1k benchmark and few-shot learning show that Convplass outperforms other PETL methods and owns remarkable domain generalization property. Our simple but effective method reveals the importance of considering the characteristics of visual tasks when designing ViT-based PETL methods, which provides a promising direction for future work.

Appendix

A Datasets

See Table 5. Since the test set of ImageNet-1k has not been released, we report its validation results in our experiments.

	Dataset	# Classes	Train	Val	Test
VTAB-1k (Zhai et al. 2019)					
Natural	CIFAR100 (Krizhevsky, Hinton et al. 2009)	100			10,000
	Caltech101 (Fei-Fei, Fergus, and Perona 2004)	102			6,084
	DTD (Cimpoi et al. 2014)	47			1,880
	Oxford-Flowers102 (Nilsback and Zisserman 2006)	102	800/1,000	200	6,149
	Oxford-Pets (Parkhi et al. 2012)	37			3,669
	SVHN (Netzer et al. 2011)	10			26,032
Specialized	Sun397 (Xiao et al. 2010)	397			21,750
	Patch Camelyon (Veeling et al. 2018)	2			32,768
	EuroSAT (Helber et al. 2019)	10	800/1,000	200	5,400
	Resisc45 (Cheng, Han, and Lu 2017)	45			6,300
Structured	Retinopathy (Kaggle and EyePacs 2015)	5			42,670
	Clevr/count (Johnson et al. 2017)	8			15,000
	Clevr/distance (Johnson et al. 2017)	6			15,000
	DMLab (Beattie et al. 2016)	6			22,735
	KITTI-Dist (Geiger et al. 2013)	4	800/1,000	200	711
	dSprites/location (Matthey et al. 2017)	16			73,728
	dSprites/orientation (Matthey et al. 2017)	16			73,728
	SmallNORB/azimuth (LeCun, Huang, and Bottou 2004)	18			12,150
	SmallNORB/elevation (LeCun, Huang, and Bottou 2004)	18			12,150
Few-shot learning					
	Food-101 (Bossard, Guillaumin, and Gool 2014)	101		20,200	30,300
	Stanford Cars (Krause et al. 2013)	196		1,635	8,041
	Oxford-Flowers102 (Nilsback and Zisserman 2006)	102	1/2/4/8/16 per class	1,633	2,463
	FGVC-Aircraft (Maji et al. 2013b)	100		3,333	3,333
	Oxford-Pets (Parkhi et al. 2012)	37		736	3,669
Domain generalization					
	ImageNet-1k (Deng et al. 2009)	1,000	16 per class	50,000	N/A
	ImageNet-V2 (Recht et al. 2019)	1,000	N/A	N/A	10,000
	ImageNet-Sketch (Wang et al. 2019)	1,000	N/A	N/A	50,889
	ImageNet-A (Hendrycks et al. 2021b)	200	N/A	N/A	7,500
	ImageNet-R (Hendrycks et al. 2021a)	200	N/A	N/A	30,000

Table 5: **Statistics of used datasets.**

B Experimental Details

B.1 Pretrained Backbones

See Table 6.

Model	Pretraining Dataset	Size (M)	Pretrained Weights
ViT-B/16 (Dosovitskiy et al. 2021)	ImageNet-21k	85.8	checkpoint
Swin-B (Liu et al. 2021b)	ImageNet-21k	86.7	checkpoint
ConvNeXt-B (Liu et al. 2022)	ImageNet-21k	87.6	checkpoint
CLIP ViT-B/16 (Radford et al. 2021)	WebImageText	85.8 (image encoder)	checkpoint

Table 6: **Pretrained backbones.**

B.2 Code Implementation

We use *PyTorch* to implement all experiments on NVIDIA RTX3090 GPUs. The implementation of models is based on *timm*.

B.3 Data Augmentation

VTAB-1k Following (Jia et al. 2022; Zhang, Zhou, and Liu 2022), we resize the images to 224×224 , and then normalize them with ImageNet’s mean and standard deviation.

Few-shot learning Following (Zhang, Zhou, and Liu 2022), for training samples, we use color-jitter and RandAugmentation; for validation/test samples, we resize them to 256×256 , crop them to 224×224 at the center, and then normalize them with ImageNet’s mean and standard deviation.

Domain generalization Following (Zhou et al. 2022), for training samples, we randomly resize and crop them to 224×224 , and then implement random horizontal flip; for validation/test samples, we resize them to 224×224 . All samples are finally normalized with ImageNet’s mean and standard deviation.

B.4 Hyperparameters

s is searched in $\{0.01, 0.1, 1, 10, 100\}$. See Table 7 for other hyperparameters.

	optimizer	learning rate	weight decay	# epochs	lr decay	# warm-up epochs
VTAB-1k	AdamW	1e-3	1e-4	100	cosine	10
Few-shot learning	AdamW	5e-3	1e-4	100	cosine	10
Domain generalization	Adam	1e-5	0	50	cosine	0

Table 7: **Hyperparameters.**

References

Ba, L. J.; Kiros, J. R.; and Hinton, G. E. 2016. Layer Normalization. *CoRR*, abs/1607.06450.

Bao, H.; Dong, L.; and Wei, F. 2022. BEiT: BERT Pre-Training of Image Transformers. In *ICLR*.

Beattie, C.; Leibo, J. Z.; Teplyashin, D.; Ward, T.; Wainwright, M.; Küttler, H.; Lefrancq, A.; Green, S.; Valdés, V.; Sadik, A.; et al. 2016. Deepmind lab. *CoRR*, abs/1612.03801.

Bossard, L.; Guillaumin, M.; and Gool, L. V. 2014. Food-101-mining discriminative components with random forests. In *ECCV*.

Brown, T. B.; Mann, B.; Ryder, N.; Subbiah, M.; Kaplan, J.; Dhariwal, P.; Neelakantan, A.; Shyam, P.; Sastry, G.; Askell, A.; Agarwal, S.; Herbert-Voss, A.; Krueger, G.; Henighan, T.; Child, R.; Ramesh, A.; Ziegler, D. M.; Wu, J.; Winter, C.; Hesse, C.; Chen, M.; Sigler, E.; Litwin, M.; Gray, S.; Chess, B.; Clark, J.; Berner, C.; McCandlish, S.; Radford, A.; Sutskever, I.; and Amodei, D. 2020. Language Models are Few-Shot Learners. *CoRR*, abs/2005.14165.

Chen, S.; Ge, C.; Tong, Z.; Wang, J.; Song, Y.; Wang, J.; and Luo, P. 2022. AdaptFormer: Adapting Vision Transformers for Scalable Visual Recognition. *CoRR*, abs/2205.13535.

Cheng, G.; Han, J.; and Lu, X. 2017. Remote Sensing Image Scene Classification: Benchmark and State of the Art. *Proc. IEEE*.

Cimpoi, M.; Maji, S.; Kokkinos, I.; Mohamed, S.; ; and Vedaldi, A. 2014. Describing Textures in the Wild. In *CVPR*.

Deng, J.; Dong, W.; Socher, R.; Li, L.-J.; Li, K.; and Fei-Fei, L. 2009. ImageNet: A large-scale hierarchical image database. In *CVPR*.

Devlin, J.; Chang, M.; Lee, K.; and Toutanova, K. 2019. BERT: Pre-training of Deep Bidirectional Transformers for Language Understanding. In *NAACL-HLT*.

Dosovitskiy, A.; Beyer, L.; Kolesnikov, A.; Weissenborn, D.; Zhai, X.; Unterthiner, T.; Dehghani, M.; Minderer, M.; Heigold, G.; Gelly, S.; Uszkoreit, J.; and Houlsby, N. 2021. An Image is Worth 16x16 Words: Transformers for Image Recognition at Scale. In *ICLR*.

Fei-Fei, L.; Fergus, R.; and Perona, P. 2004. Learning generative visual models from few training examples: An incremental bayesian approach tested on 101 object categories. In *CVPR workshop*.

Geiger, A.; Lenz, P.; Stiller, C.; and Urtasun, R. 2013. Vision meets robotics: The kitti dataset. *The International Journal of Robotics Research*.

He, J.; Zhou, C.; Ma, X.; Berg-Kirkpatrick, T.; and Neubig, G. 2022a. Towards a Unified View of Parameter-Efficient Transfer Learning. In *ICLR*.

He, K.; Chen, X.; Xie, S.; Li, Y.; Dollár, P.; and Girshick, R. B. 2022b. Masked Autoencoders Are Scalable Vision Learners. In *CVPR*.

He, K.; Zhang, X.; Ren, S.; and Sun, J. 2016. Deep Residual Learning for Image Recognition. In *CVPR*.

Helber, P.; Bischke, B.; Dengel, A.; and Borth, D. 2019. Eu-rosat: A novel dataset and deep learning benchmark for land use and land cover classification. *IEEE Journal of Selected Topics in Applied Earth Observations and Remote Sensing*.

Hendrycks, D.; Basart, S.; Mu, N.; Kadavath, S.; Wang, F.; Dorundo, E.; Desai, R.; Zhu, T.; Parajuli, S.; Guo, M.; Song, D.; Steinhardt, J.; and Gilmer, J. 2021a. The Many Faces of Robustness: A Critical Analysis of Out-of-Distribution Generalization. In *ICCV*.

Hendrycks, D.; Zhao, K.; Basart, S.; Steinhardt, J.; and Song, D. 2021b. Natural Adversarial Examples. In *CVPR*.

Houlsby, N.; Giurgiu, A.; Jastrzebski, S.; Morrone, B.; de Laroussilhe, Q.; Gesmundo, A.; Attariyan, M.; and Gelly, S. 2019. Parameter-Efficient Transfer Learning for NLP. In *ICML*.

Hu, E. J.; yelong shen; Wallis, P.; Allen-Zhu, Z.; Li, Y.; Wang, S.; Wang, L.; and Chen, W. 2022. LoRA: Low-Rank Adaptation of Large Language Models. In *ICLR*.

Jia, M.; Tang, L.; Chen, B.; Cardie, C.; Belongie, S. J.; Hariharan, B.; and Lim, S. 2022. Visual Prompt Tuning. In *ECCV*.

Johnson, J.; Hariharan, B.; Van Der Maaten, L.; Fei-Fei, L.; Lawrence Zitnick, C.; and Girshick, R. 2017. Clevr: A diagnostic dataset for compositional language and elementary visual reasoning. In *CVPR*.

Kaggle; and EyePacs. 2015. Kaggle diabetic retinopathy detection.

Kolesnikov, A.; Beyer, L.; Zhai, X.; Puigcerver, J.; Yung, J.; Gelly, S.; and Houlsby, N. 2020. Big Transfer (BiT): General Visual Representation Learning. In *ECCV*.

Krause, J.; Stark, M.; Deng, J.; and Fei-Fei, L. 2013. 3d object representations for fine-grained categorization. In *CVPR workshops*.

Krizhevsky, A.; Hinton, G.; et al. 2009. Learning multiple layers of features from tiny images.

LeCun, Y.; Huang, F. J.; and Bottou, L. 2004. Learning methods for generic object recognition with invariance to pose and lighting. In *CVPR*.

Li, X. L.; and Liang, P. 2021. Prefix-Tuning: Optimizing Continuous Prompts for Generation. In *ACL/IJCNLP*.

Liu, X.; Ji, K.; Fu, Y.; Du, Z.; Yang, Z.; and Tang, J. 2021a. P-Tuning v2: Prompt Tuning Can Be Comparable to Fine-tuning Universally Across Scales and Tasks. *CoRR*, abs/2110.07602.

Liu, Z.; Lin, Y.; Cao, Y.; Hu, H.; Wei, Y.; Zhang, Z.; Lin, S.; and Guo, B. 2021b. Swin Transformer: Hierarchical Vision Transformer using Shifted Windows. In *ICCV*.

Liu, Z.; Mao, H.; Wu, C.; Feichtenhofer, C.; Darrell, T.; and Xie, S. 2022. A ConvNet for the 2020s. In *CVPR*.

Maji, S.; Rahtu, E.; Kannala, J.; Blaschko, M.; and Vedaldi, A. 2013a. Fine-grained visual classification of aircraft. *CoRR*, abs/1306.5151.

Maji, S.; Rahtu, E.; Kannala, J.; Blaschko, M. B.; and Vedaldi, A. 2013b. Fine-Grained Visual Classification of Aircraft. *CoRR*, abs/1306.5151.

Matthey, L.; Higgins, I.; Hassabis, D.; and Lerchner, A. 2017. dsprites: Disentanglement testing sprites dataset.

Netzer, Y.; Wang, T.; Coates, A.; Bissacco, A.; Wu, B.; and Ng, A. Y. 2011. Reading digits in natural images with unsupervised feature learning.

Nilsback, M.-E.; and Zisserman, A. 2006. A visual vocabulary for flower classification. In *CVPR*.

Park, N.; and Kim, S. 2022. How Do Vision Transformers Work? In *ICLR*.

Parkhi, O. M.; Vedaldi, A.; Zisserman, A.; and Jawahar, C. 2012. Cats and dogs. In *CVPR*.

Pfeiffer, J.; Kamath, A.; Rücklé, A.; Cho, K.; and Gurevych, I. 2021. AdapterFusion: Non-Destructive Task Composition for Transfer Learning. In *EACL*.

Radford, A.; Kim, J. W.; Hallacy, C.; Ramesh, A.; Goh, G.; Agarwal, S.; Sastry, G.; Askell, A.; Mishkin, P.; Clark, J.; Krueger, G.; and Sutskever, I. 2021. Learning Transferable Visual Models From Natural Language Supervision. In *ICML*, Proceedings of Machine Learning Research.

Raffel, C.; Shazeer, N.; Roberts, A.; Lee, K.; Narang, S.; Matena, M.; Zhou, Y.; Li, W.; and Liu, P. J. 2020. Exploring the Limits of Transfer Learning with a Unified Text-to-Text Transformer. *J. Mach. Learn. Res.*, 21: 140:1–140:67.

Recht, B.; Roelofs, R.; Schmidt, L.; and Shankar, V. 2019. Do ImageNet Classifiers Generalize to ImageNet? In *ICML*.

Vaswani, A.; Shazeer, N.; Parmar, N.; Uszkoreit, J.; Jones, L.; Gomez, A. N.; Kaiser, L.; and Polosukhin, I. 2017. Attention is All you Need. In *NIPS*.

Veeling, B. S.; Linmans, J.; Winkens, J.; Cohen, T.; and Welling, M. 2018. Rotation Equivariant CNNs for Digital Pathology. *CoRR*, abs/1806.03962.

Veit, A.; Wilber, M. J.; and Belongie, S. J. 2016. Residual Networks Behave Like Ensembles of Relatively Shallow Networks. In *NIPS*.

Wang, H.; Ge, S.; Lipton, Z. C.; and Xing, E. P. 2019. Learning Robust Global Representations by Penalizing Local Predictive Power. In *NeurIPS*.

Wang, W.; Bao, H.; Dong, L.; and Wei, F. 2021. VLMo: Unified Vision-Language Pre-Training with Mixture-of-Modality-Experts. *CoRR*, abs/2111.02358.

Wu, H.; Xiao, B.; Codella, N.; Liu, M.; Dai, X.; Yuan, L.; and Zhang, L. 2021. CvT: Introducing Convolutions to Vision Transformers. In *ICCV*.

Xiao, J.; Hays, J.; Ehinger, K. A.; Oliva, A.; and Torralba, A. 2010. Sun database: Large-scale scene recognition from abbey to zoo. In *CVPR*.

Yu, J.; Wang, Z.; Vasudevan, V.; Yeung, L.; Seyedhosseini, M.; and Wu, Y. 2022. CoCa: Contrastive Captioners are Image-Text Foundation Models. *CoRR*, abs/2205.01917.

Zhai, X.; Kolesnikov, A.; Houlsby, N.; and Beyer, L. 2022. Scaling vision transformers. In *CVPR*.

Zhai, X.; Puigcerver, J.; Kolesnikov, A.; Ruyssen, P.; Riquelme, C.; Lucic, M.; Djolonga, J.; Pinto, A. S.; Neumann, M.; Dosovitskiy, A.; Beyer, L.; Bachem, O.; Tschannen, M.; Michalski, M.; Bousquet, O.; Gelly, S.; and Houlsby, N. 2019. The Visual Task Adaptation Benchmark. *CoRR*, abs/1910.04867.

Zhang, Y.; Zhou, K.; and Liu, Z. 2022. Neural Prompt Search. *CoRR*, abs/2206.04673.

Zhou, K.; Yang, J.; Loy, C. C.; and Liu, Z. 2021. Learning to Prompt for Vision-Language Models. *CoRR*, abs/2109.01134.

Zhou, K.; Yang, J.; Loy, C. C.; and Liu, Z. 2022. Conditional Prompt Learning for Vision-Language Models. In *CVPR*.